Nastaran Khodabandehloo
Department of Mechanical Engineering,
University of Houston,
Houston, TX 77204
e-mail: khd.nastaran@gmail.com

Kosar Mozaffari
Department of Mechanical Engineering,
University of Houston,
Houston, TX 77204
e-mail: mozaffari.kosar@gmail.com

Liping Liu[1]
Department of Mathematics and Mechanical and Aerospace Engineering,
Rutgers University,
NJ 08854
e-mail: liu.liping@rutgers.edu

Pradeep Sharma[1]
Department of Mechanical Engineering and Physics,
University of Houston,
Houston, TX 77204
e-mails: psharma@uh.edu;
psharma@central.uh.edu

Micro-Structural Design of Soft Solid Composite Electrolytes With Enhanced Ionic Conductivity

Electrolyte in a rechargeable Li-ion battery plays a critical role in determining its capacity and efficiency. While the typically used electrolytes in Li-ion batteries are liquid, soft solid electrolytes are being increasingly explored as an alternative due to their advantages in terms of increased stability, safety and potential applications in the context of flexible and stretchable electronics. However, ionic conductivity of solid polymer electrolytes is significantly lower compared to liquid electrolytes. In a recent work, we developed a theoretical framework to model the coupled deformation, electrostatics and diffusion in heterogeneous electrolytes and also established a simple homogenization approach for the design of microstructures to enhance ionic conductivity of composite solid electrolytes. Guided by the insights from the theoretical framework, in this paper, we examine specific microstructures that can potentially yield significant improvement in the effective ionic conductivity. We numerically implement our theory in the open source general purpose finite element package FEniCS *to solve the governing equations and present numerical solutions and insights on the effect of microstructure on the enhancement of ionic conductivity. Specifically, we investigate the effect of shape by considering ellipsoidal inclusions. We also propose an easily manufacturable microstructure that increases the ionic conductivity of the composite electrolyte by 40 times, simply by the addition of dielectric columns parallel to the solid electrolyte phase.* [DOI: 10.1115/1.4053498]

Keywords: sustainable energy, ionic conductivity, solid-state electrolyte, Li-ion battery, finite element analysis, constitutive modeling of materials, micromechanics

1 Introduction

Rechargeable Li-ion batteries are expected to play a central role in the future of energy storage—be it in the context of consumer electronics, or sustainable vehicles [1,2]. The ramifications (and need) for renewable energy, and the critical role energy storage will play in that context, hardly needs much discussion due to the extensive public discourse on the topic and extensive scientific research [3,4]. Germane to this, scientific research has focused on both fundamental science as well as the designing the relevant materials and motifs to engineer efficient, higher energy density, and safer batteries [5–7].

A typical Li-ion battery consists of several electrochemical cells connected in series or in parallel. The three primary components of the cell are a negatively charged electrode (cathode), its counterpart—the anode, and an intervening electrolyte that enables ion transfer between the two electrodes. The ionic conductivity of an electrolyte quantifies how mobile and available the ions are in an electrolyte [8] and, in addition to other aspects such as the design and chemistry of the electrodes, plays a critical role in the determination of the power output of the cell [9]. An electrolyte should ideally be both an excellent ionic conductor *and* electronic insulator; so that ion transport can be facile and self-discharge is kept to a minimum [10].

Conventionally, electrolytes are liquid. However, increasingly, solid electrolytes are being considered as alternatives. Liquid electrolytes are extremely flammable and a battery containing liquid electrolyte can be a fire hazard in case of over-charging or short-circuiting [11]. In contrast, solid electrolytes are thermally stable. Furthermore, liquid electrolytes exhibit a greater propensity for uncontrollable dendritic growth [12], which can cause short circuit conditions [13]. Finally, due to the growing interest in stretchable and flexible electronics, there is a strong impetus to develop soft solid electrolytes that can integrate with such electronic devices [14–20].

Despite all the advantages that soft (polymer-based) solid electrolytes offer, their ionic conductivity is significantly lower than their widely used liquid counterparts [21]. To that end, several approaches have been proposed to increase the ionic conductivity in polymer electrolytes.[2] As an example, a common method to ameliorate ionic conductance is the addition of plasticizers which reduces the crystalline nature of the polymer matrix and can increase the ion mobility of the structure [22]. However, mechanical properties may be compromised (i.e., mechanical stability) [23].

Another strategy involves creating composite electrolytes by embedding nanofillers in a polymer matrix [22,25–27]. Using such an approach, Croce and co-workers demonstrated a significant enhancement in ionic conductivity [28]. Interestingly, some works have also shown a *decrease* in ionic conductivity with the addition of nanofillers—e.g., Weston and Steele reported no effect in ionic conductivity by addition of Al_2O_3 and even reduction in ionic conductivity at high volume fractions [29]. The enhancement of ionic conductivity because of addition of nanofillers was attributed to the formation of a spherulite structure in the interphase region of the matrix-inclusion which consists of both highly crystalline structure and amorphous region (as shown in Fig. 1). This region possesses a much higher ion mobility compared to the polymer electrolyte [30]. Recent studies have also shown that the addition of nano-scale highly conductive inorganic particulate fillers into polymer electrolytes can not only significantly enhance the ionic

[1]Corresponding authors.

Contributed by the Applied Mechanics Division of ASME for publication in the Journal of Applied Mechanics. Manuscript received January 1, 2022; final manuscript received January 6, 2022; published online February 11, 2022. Assoc. Editor: Yonggang Huang.

[2]Ionic conductivity is not the only feature of the electrolyte that is important to battery effectiveness. The operating voltage range, thermal stability among others aspects are also of interest. Our work, however, is primarily focused on the improvement of ionic conductivity.

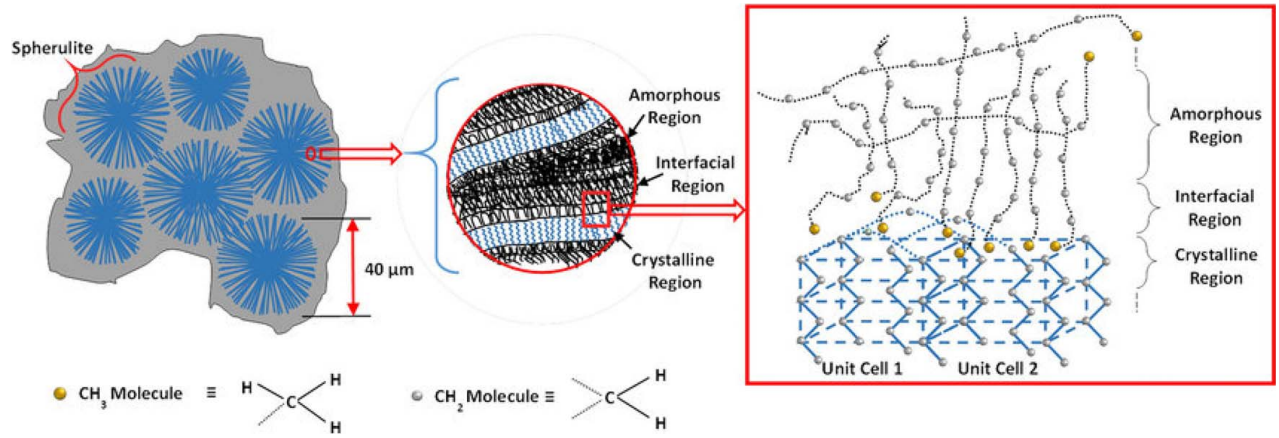

Fig. 1 Schematic of the spherulite structure. The figure is from Ref. [24]. Reprinted with the permission of AIP Publishing.

conductivity of the electrolytes but also improve its mechanical strength and stability [31]. Finally, mechanical deformation has also been found to strongly influence ionic conductivity of polymer electrolytes [18,32,33]. A linear relation between ionic conductivity was found by Ref. [33] (for up to 15% strain leading to 400% improvement in ionic conductivity). This trend was also confirmed by our previous theoretical work [34] predicated on small-deformation theory.

Complementary to experimental efforts (some of which we have cited in the preceding paragraphs), several theoretical and computational works have also appeared to study the coupled effect of deformation, ionic diffusion, and electrostatics. Specifically in the mechanics community, different groups have approached the theory of electrolytes in slightly different manners and often with a different emphasis, or even for applications other than batteries (e.g., ferroelectrics, polymer-metal actuators) [35–44]. The first paper (that we know off) that proposed homogenization to design composite electrolytes specific to the context of batteries is arguably that of Sillamoni and Idiart [45]. Very recently, we also proposed [34] a theoretical framework to address the coupling of electrostatics, ionic diffusion, and deformation in composite electrolytes. In particular, we presented a simple homogenization procedure that allows the simplification of the rather complicated nonlinear problem and reconciled the various experimental observations in the literature. In our prior work, the approach was almost entirely analytical which limited the modeling to simple microstructures. Guided and inspired by the insights of our prior work, in this paper, we undertake a computational study to understand the effect of some specific microstructures on the possibility of designing enhanced ionic conductivity. Specifically, we (i) implement the pertinent governing equations in the open-source code of *FEniCS*; (ii) analyze composite electrolytes with ellipsoidal inclusions to understand the effect of shape effects on ion conductivity enhancement; (iii) analyze the effect of size of embedded inclusions; (iv) determine the effect of finite deformation on the effective ionic conductivity of electrolytes—we remark that our prior work, due to its analytical nature, focused on small-deformation, and (v) propose a specific, easily manufacturable, microstructure that can yield a significant enhancement in ionic conductivity.

This paper is organized as follows, in Sec. 2, we briefly summarize the theoretical framework. In Sec. 3, we present the relevant details related to the computational procedure and provide benchmark solutions in Sec. 4. We discuss shape effects in Sec. 5, the effect of deformation on ionic conductivity in Sec. 6 and our proposal of a new microstructure in Sec. 7.

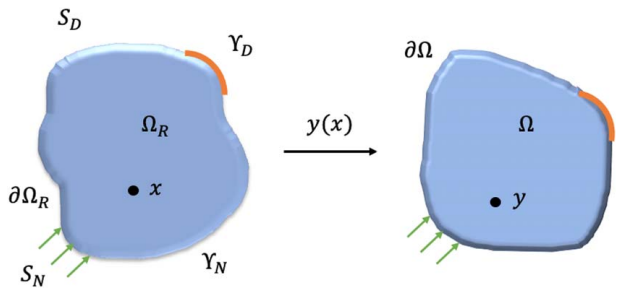

Fig. 2 An ionic-conductive electro-elastic-diffusive body in reference and current configuration subject to external mechanical traction on S_N, prescribed displacement on S_D where $S_D = \partial\Omega/S_N$. The system is connected to a solution of ions in Υ_D and directional flux perpendicular to the boundary on Υ_N is prescribed where $\Upsilon_N = \partial\Omega/\Upsilon_D$. The prescribed boundary electric potential is also defined on Ω_R where the electrolyte is subjected to an electric potential difference.

2 Theoretical Framework

In this section, we briefly summarize the mathematical model of an electro-elastic-diffusive system in an electrolyte we presented in Ref. [34]. Consider Fig. 2, where we assume that the thermodynamic state of the system is described by deformation $y(0, t)$: $\Omega_R \to \Omega(t)$, ionic volumetric concentration $c(0, t) : \Omega_R \to \mathbb{R}$, and the electric potential $\xi : \Omega_R \to \mathbb{R}$ in the reference configuration. The deformation gradient, Cauchy-Green tensor, and the Jacobian are denoted by

$$\mathbf{F} = \nabla \mathbf{y}, \quad \mathbf{C} = \mathbf{F}^T\mathbf{F}, \quad J = \det\nabla \mathbf{y} \tag{1}$$

Work can be done on the chemo-mechanical-electrical system body through the following boundary conditions:

- Mechanical boundary conditions:

$$\begin{cases} \mathbf{y}(\mathbf{x}, t) = \mathbf{y}_b(\mathbf{x}, t) & \text{on} \quad S_D \\ \text{applied external traction} = \mathbf{t}^e(\mathbf{x}, t) & \text{on} \quad S_N \end{cases} \tag{2}$$

  where $\mathbf{y}_b(0, t) : S_D \to \mathbb{R}^3$ is the prescribed boundary position and S_D and S_N (as shown in Fig. 2) are the subdivisions of $\partial\Omega$.
- Electrical boundary conditions:

$$\xi = \xi^e(\mathbf{x}) \quad \text{on} \quad \partial\Omega_R \tag{3}$$

  where $\xi^e(\mathbf{x})$ is prescribed boundary electric potential on $\partial\Omega_R$ which is controlled by an external circuit.
- Chemical boundary conditions:

$$\begin{cases} \mu = \mu^e(\mathbf{x},t) & \text{on} \quad \Upsilon_D \\ \mathbf{J} \cdot \mathbf{n} = \mathbf{J}^e & \text{on} \quad \Upsilon_N \end{cases} \tag{4}$$

where $\mu^e(0,t):\Upsilon_D \to \mathbb{R}$ is the prescribed boundary chemical potential which is usually dictated by the materials of active electrodes, and $\mathbf{J}(0,t):\Omega_R \to \mathbb{R}^3$ is the ionic flux. Also, Υ_D and Υ_N are another subdivisions of $\partial\Omega$.

By the conservation law of ions, we have

$$\dot{c} + \nabla \cdot \mathbf{J} = 0 \quad \text{in} \quad \Omega_R \tag{5}$$

The external system does work on the body by mechanical traction, transportation of ions across the boundary and the applied electric voltage from the electrodes. The rate of work done on the continuum body is [34]

$$\dot{W} = \int_{\partial\Omega_R} \dot{\mathbf{y}} \cdot \mathbf{t}^e - \int_{\partial\Omega_R} (\mu_e + q\xi_e)(\mathbf{J}\cdot\mathbf{n}) - \int_{\partial\Omega_R} \xi(\dot{\tilde{\mathbf{D}}}\cdot\mathbf{n}) \tag{6}$$

where q is the electric charge associated with each mobile ion and as a result the electric current density is given by $\mathbf{J}_e = q\mathbf{J}$. Also, $\tilde{\mathbf{D}} = -\epsilon(\mathbf{x})\mathbf{J}\mathbf{C}^{-1}\nabla\xi$ is the nominal electric displacement.[3]

To achieve a closed differential system governing the electro-elastic-diffusion of the body we need to propose the free energy of the body.

In equilibrium state, we assume the free energy of the body to be specified by

$$\begin{aligned} U(\mathbf{y},c) &= U_b(\mathbf{y},c) + U_e \\ U_b(\mathbf{y},c) &= \int_{\Omega_R} \Psi(\nabla\mathbf{y}, c) \end{aligned} \tag{7}$$

where $\Psi:\mathbb{R}^{3\times3}\times\mathbb{R}\to\mathbb{R}$ is the free energy density and U_e is the electric energy associated with charges and polarization. For simplicity, we assume that the material is isotropic so the rate of change of free energy of the body in isothermal process is given by

$$\dot{U}_b = \frac{\mathrm{d}}{\mathrm{d}t}\int_{\Omega_R} \Psi(\nabla\mathbf{y}, c) = \int_{\Omega_R}\left[\frac{\partial\Psi(\mathbf{F},c)}{\partial\mathbf{F}}\cdot\nabla\dot{\mathbf{y}} + \frac{\partial\Psi(\mathbf{F},c)}{\partial c}\dot{c}\right] \tag{8}$$

For brevity, we define the following terms:

$$\begin{aligned} \mathbf{P} &:= D_F\Psi(\nabla\mathbf{y}, c) = \frac{\partial\Psi(\mathbf{F},c)}{\partial\mathbf{F}} \\ \mu &:= D_c\Psi(\nabla\mathbf{y}, c) = \frac{\partial\Psi(\mathbf{F},c)}{\partial c} \end{aligned} \tag{9}$$

By substituting them in Eq. (8) and using the conservation law of ions presented in Eq. (5), we rewrite the equation as follows:

$$\dot{U}_b = \int_{\Omega_R} [\mathbf{P}\cdot\nabla\dot{\mathbf{y}} - \mu\nabla\cdot\mathbf{J}] \tag{10}$$

Neglecting dynamical effects, the electric field in reference configuration satisfies the Maxwell equations:

$$\mathrm{div}\tilde{\mathbf{D}} = \mathrm{div}(-\epsilon(\mathbf{x})\mathbf{J}\mathbf{C}^{-1}\nabla\xi) = q(c - c_0(\mathbf{x})) \quad \text{in } \Omega_R \tag{11}$$

where $\epsilon(\mathbf{x})$ is the electric permittivity and $c_0:\Omega_R\to\mathbb{R}$ is the immobile ion concentration that would neutralize the mobile ions in a natural equilibrium state. For simplicity, we also assume that the electric permittivity itself is independent of deformation. Therefore, polarization in current configuration can be defined by $\mathbf{p} = -(\epsilon - \epsilon_0)\nabla_{\mathbf{y}}\xi$ in which ϵ_0 is the vacuum permittivity. Hence, the electrical energy stored in the system (U_e) is defined as follows:

$$U_e[\mathbf{y}, c] = \int_{\Omega_R}\left[\frac{\epsilon_0}{2}|\nabla_{\mathbf{y}}\xi|^2 + \frac{|\mathbf{p}|^2}{2(\epsilon(\mathbf{x}) - \epsilon_0)}\right] \tag{12}$$

With a bit of technical calculation, the final form of rate of change of electrical energy(U_e) [35], can be written as

$$\dot{U}_e[\mathbf{y}, c] = \int_{\Omega_R}[-\dot{\mathbf{y}}\cdot\mathrm{div}\Sigma_{MW} + \mathbf{J}\cdot\nabla(q\xi)] + \int_{\Omega_R}\dot{\mathbf{y}}\cdot(\Sigma_{MW})\mathbf{n} \tag{13}$$

where Σ_{MW} is identified as the Piola–Maxwell stress and is denoted as

$$\Sigma_{\mathrm{MW}}(\mathbf{x}) = -\frac{\epsilon(\mathbf{x})}{2}J|\mathbf{F}^{-\mathrm{T}}\nabla\xi|^2\mathbf{F}^{-\mathrm{T}} + \epsilon(\mathbf{x})J(\mathbf{F}^{-\mathrm{T}}\nabla\xi)\otimes(\mathbf{F}^{-\mathrm{T}}\nabla\xi) \tag{14}$$

From Eqs. (6), (10), and (13). The rate of energy dissipation is written as

$$\begin{aligned} \dot{D} &= \dot{W} - \dot{U} = \dot{W} - \dot{U}_b - \dot{U}_e \\ &= \int_{\partial\Omega_R}\dot{\mathbf{y}}\cdot\mathbf{t}^e - \int_{\partial\Omega_R}(\mu_e + q\xi_e)(\mathbf{J}\cdot\mathbf{n}) \\ &\quad + \int_{\Omega_R}[\mathrm{div}(\mathbf{P}+\Sigma_{MW})\cdot\dot{\mathbf{y}} - \mathbf{J}\nabla\cdot(\mu + q\xi)] \\ &\quad + \int_{\partial\Omega_R}[-\dot{\mathbf{y}}\cdot(\mathbf{P}+\Sigma_{MW})\mathbf{n} + (\mathbf{J}\cdot\mathbf{n})(\mu + q\xi)] \geq 0 \end{aligned} \tag{15}$$

The inequality is from the second law of thermodynamics—the rate of energy dissipation must always be a positive value ($\dot{D} \geq 0$).

Using the standard Coleman–Noll procedure, the following may be concluded:

- Non-negative rate of dissipation:

$$-\mathbf{J}\cdot\nabla(\mu + q\xi) \geq 0 \tag{16}$$

- Interior mechanical balance:

$$\mathrm{div}(\mathbf{P} + \Sigma_{MW}) = 0 \quad \text{in } \Omega_R \tag{17}$$

- Boundary conditions:

$$(\mathbf{P} + \Sigma_{MW})\mathbf{n} - \mathbf{t}^e = 0 \quad \text{on } S_N \tag{18}$$

and

$$\begin{cases} \mu^e + q\xi^e = \mu + q\xi & \text{on} \quad \Upsilon_D \\ \mathbf{J}\cdot\mathbf{n} = 0 & \text{on} \quad \Omega_R\backslash\Upsilon_D \end{cases} \tag{19}$$

By Eq. (16), a constitutive response that is consistent with the second law of thermodynamics (and arguably represents the simplest choice we can make) is linear mobility/diffusion:

$$\mathbf{v} = -\gamma(\mathbf{x})\nabla(\mu + q\xi), \quad \mathbf{J} = c\mathbf{v} \quad \text{in} \quad \Omega_R \tag{20}$$

where $\gamma(\mathbf{x})$ represents the ionic mobility of the material.

In this work, we will consider both finite and infinitesimal deformation to understand not only the effect of deformation but also the importance (or not) of accounting for large deformation behavior. For a linearized theory, we expand the free energy density at a reference equilibrium state as follows:

$$\begin{aligned} \Psi(\mathbf{F}, c; \mathbf{x}) \approx{}& \frac{1}{2}(\mathbf{F}-\mathbf{I})\cdot\mathbb{C}(\mathbf{x})(\mathbf{F}-\mathbf{I}) + \alpha_{\mathrm{el}}(c - c_0(\mathbf{x}))\mathrm{Tr}(\mathbf{F}-\mathbf{I}) \\ &+ \frac{\beta(\mathbf{x})}{2}(c - c_0(\mathbf{x}))^2 + \hat{\mu}(\mathbf{x})(c - c_0(\mathbf{x})) + \Psi(\mathbf{I}, c_0; \mathbf{x}) \end{aligned} \tag{21}$$

where $\mathbf{I}$ is the identity matrix, $\hat{\mu}$ denotes the chemical potential for pure ion, and $\mathbb{C}$ is the forth-order elasticity tensor.

In the case of infinitesimal deformation, the complete coupled system of governing equations for $(\mu, \xi, \mathbf{u})$ using Eq. (21) can

[3]We remark that the presence of charge diffusion in a continuum body also relates to the so-called electret materials except that in the latter, the charges are "frozen" and convect with deformation in the time-scale of interest [46–48].

now be written as

$$\begin{cases} \nabla\cdot(-\epsilon_r\nabla\xi)+\frac{q^2}{\epsilon_0\beta}\xi=\frac{q}{\epsilon_0\beta}(\mu+q\xi-\hat{\mu}-\alpha_{\rm el}\nabla\cdot\mathbf{u}) & \text{in } \Omega_R \\ \nabla\cdot\left[\mathbb{C}\nabla\mathbf{u}+\frac{\alpha_{el}}{\beta}(\mu-\hat{\mu}-\alpha_{\rm el}\nabla\cdot\mathbf{u})\mathbf{I}\right]=0 & \text{in } \Omega_R \\ \nabla\cdot[-\gamma c\nabla(\mu+q\xi)]=\dot{c}, \quad c-c_0=\frac{(\mu-\hat{\mu}-\alpha_{\rm el}\nabla\cdot\mathbf{u})}{\beta} & \text{in } \Omega_R \end{cases} \tag{22}$$

To account for deformation nonlinearity, we will consider an incompressible neo-Hookean material. However, we also note that the permeation of charged ions (or uncharged molecules) induces significant volume change of the material. To model this phenomenon, we may enforce a kinematic constraint:

$$\Phi(\mathbf{F},c)=\det\mathbf{F}-(1+\nu_i(c-c_0))=0 \tag{23}$$

where ν_i can be interpreted as volume of ions [34]. Accounting for the constraint, the free energy density of the body Ω_R can be written as

$$\Psi(\mathbf{F},c)=\frac{1}{2}G(|\mathbf{F}|^2-3)+\frac{\beta}{2}(c-c_0)^2+\hat{\mu}(c-c_0)-\Pi\Phi(\mathbf{F},c) \tag{24}$$

where G is the shear modulus. So the governing equations then become:

$$\begin{cases} \nabla\cdot(-\epsilon_r\nabla\xi)+\frac{q^2}{\epsilon_0\beta}\xi=\frac{q}{\epsilon_0\beta}(\mu+q\xi-\hat{\mu}-\Pi\nu_i) & \text{in} \quad \Omega_R \\ \nabla\cdot[\mathbf{P}+\mathbf{\Sigma}_{MW}]=0 & \text{in} \quad \Omega_R \\ \nabla\cdot[(-\gamma c\nabla(\mu+q\xi)]=\dot{c}, \quad c-c_0=\frac{(\mu-\hat{\mu}-\Pi\nu_i)}{\beta} & \text{in} \quad \Omega_R \end{cases} \tag{25}$$

where $\mathbf{P}=G\mathbf{F}-J\Pi\mathbf{F}^{-T}$.

To demonstrate the fundamental behavior of the system in Eqs. (22) and (25) and analyze the homogenization of composite electrolytes, we consider a one-dimensional and homogeneous electrolyte body between two charge collectors $\Delta\xi=\xi_1-\xi_0$. We also introduce the electro-chemical potential by

$$\Phi=\mu+q\xi \tag{26}$$

and Debye length as the screening length for electrostatic interactions[4]

$$\lambda=\sqrt{\frac{\epsilon_0\beta}{q^2}} \tag{27}$$

Taking cognizance of the relation between the ionic flux J and the external electrical current $I=qJA$, the ionic conductivity of electrolyte must satisfy the following equation:

$$J=-K\frac{\Delta\phi}{d} \tag{28}$$

where ϕ is the electro-chemical potential and defined as $\phi=\mu+q\xi$ [34]. The electric potential difference between the electrodes satisfies Ohm's law $\Delta\xi=IR=qJAR$.

To facilitate the interpretation of ionic conductivity, consider one-dimensional ion transport in a non-equilibrium process where $J\neq0$ and in the steady-state limit of Eq. (22). In that case, we have the following relation for the electrochemical potential difference:

$$\Delta\phi=\phi_1-\phi_0=-\frac{Jd}{K}=-\int_0^d\frac{J}{\gamma c(x)}\,\mathrm{d}x=-\int_0^d\frac{J}{\gamma(c+\hat{c})}\,\mathrm{d}x \tag{29}$$

where $\hat{c}$ is the change of concentration due to ion transportation. Assuming the change of concentration of ions is mostly due to the chemical potential difference at the boundaries [34], we can safely neglect $\hat{c}$ and rewrite Eq. (29) as below,

$$\phi'=\frac{J}{\gamma(c+\hat{c})}\approx\frac{J}{\gamma c}\rightarrow\Delta\phi\approx-J\int_0^d\frac{1}{\gamma c(x)}\,\mathrm{d}x \tag{30}$$

Therefore, using Eq. (28), the ionic conductivity K in one-dimension can be defined as,

$$K=\left[\frac{1}{d}\int_0^D\frac{1}{\gamma c(x)}\,\mathrm{d}x\right]^{-1} \tag{31}$$

where $c(x)$ is the equilibrium ionic concentration obtained from solving Eq. (22) in the steady-state limit.

3 Finite Element Implementation

The governing partial differential equations for the chemo-electro-mechanical system derived in the preceding section are rather difficult to solve except for some very simple cases. In this section, we described the finite element implementation to solve these numerically.

3.1 Dimensionless Form of the Governing Equations. As a first step to derive the corresponding weak form of the coupled system of partial differential equations, we non-dimensionalize them to simplify the calculations and facilitate eventual physical interpretation. As evident, three primary variables are involved: (ξ, μ, $\mathbf{u}$). The dimensionless parameters are presented,

$$\begin{aligned} &\bar{\xi}=\frac{\xi q}{\mu_{\rm ref}}, \quad \bar{\mathbf{u}}=\frac{\mathbf{u}}{H}, \quad \bar{\mu}=\frac{\mu}{\mu_{\rm ref}}, \quad \bar{c}=\frac{c}{c_{\rm ref}} \\ &\bar{t}=\frac{t}{T}, \quad \left(T=\frac{\mu_{\rm ref}\gamma_{\rm ref}}{H^2}\right) \\ &\bar{\beta}=\frac{\beta c_{\rm ref}^2}{G_{\rm ref}}, \quad \bar{\hat{\mu}}=\frac{\hat{\mu}}{\mu_{\rm ref}}, \quad \bar{c}_0=\frac{c_0}{c_{\rm ref}} \\ &\bar{\gamma}=\frac{\gamma}{\gamma_{\rm ref}}, \quad \bar{\alpha}_{\rm el}=\frac{\alpha_{\rm el}c_{\rm ref}}{G_{\rm ref}}, \quad \bar{\nabla}=H\nabla \end{aligned} \tag{32}$$

where H and T are the non-dimensionalization parameters associated with the smallest length scale and the time scale, respectively, and G is the shear modulus. Also, $c_{\rm ref}$, $\mu_{\rm ref}$, $G_{\rm ref}$, and $\gamma_{\rm ref}$ are the normalization factors associated with the primary variables. For simplicity, we set $c_{\rm ref}=c_0$, $\mu_{\rm ref}=\hat{\mu}$, $G_{\rm ref}=G$, and $\gamma_{\rm ref}=\gamma$ for the homogeneous electrolyte. With this, the governing equations in dimensionless form are as follows:

$$\bar{\nabla}\cdot(-\epsilon_r\bar{\nabla}\bar{\xi})-\frac{\Phi^2}{\bar{\beta}}(\bar{\mu}-\bar{\hat{\mu}})+\frac{\bar{\alpha}_{\rm el}}{\bar{\beta}}\frac{\Phi^2}{\Gamma}\bar{\nabla}\cdot\bar{\mathbf{u}}=0 \tag{33}$$

$$\bar{\nabla}\cdot\left[\frac{\mathbb{C}}{G_{\rm ref}}\bar{\nabla}\bar{\mathbf{u}}+\bar{\alpha}_{\rm el}\frac{\Gamma}{\bar{\beta}}(\bar{\mu}-\bar{\hat{\mu}})\mathbf{I}-\frac{\bar{\alpha}_{\rm el}{}^2}{\bar{\beta}}\bar{\nabla}\cdot\bar{\mathbf{u}}\mathbf{I}\right]=0 \tag{34}$$

$$\begin{aligned} &\bar{\nabla}\cdot\left[-\bar{\gamma}\left(\frac{\Gamma}{\bar{\beta}}(\bar{\mu}-\bar{\hat{\mu}})-\bar{\nabla}\cdot\bar{\mathbf{u}}\frac{\bar{\alpha}_{\rm el}}{\bar{\beta}}+\bar{c}_0\right)\bar{\nabla}(\bar{\mu}+\bar{\xi})\right] \\ &=\frac{H^2}{\mu_{\rm ref}\gamma_{\rm ref}}\frac{1}{T}\frac{\mathrm{d}}{\mathrm{d}\bar{t}}\left(\frac{\Gamma}{\bar{\beta}}(\bar{\mu}-\bar{\hat{\mu}})-\bar{\nabla}\cdot\mathbf{u}\frac{\bar{\alpha}_{\rm el}}{\bar{\beta}}+\bar{c}_0\right) \end{aligned} \tag{35}$$

where $\Phi=Hqc_{\rm ref}/\sqrt{\epsilon_0 G_{\rm ref}}$ and $\Gamma=\mu_{\rm ref}c_{\rm ref}/G_{\rm ref}$.

For the neo-Hookean case presented in Eq. (25), the additional dimensionless parameters are

$$\bar{\nu}_i=\nu_i c_{\rm ref}, \quad \bar{\Pi}=\frac{\Pi}{G_{\rm ref}} \tag{36}$$

[4]The *conventional* homogenization of the conductivity problem (predicated on the classical Poisson equation) is size-independent. However, in the current framework, due to the presence of the Debye length, there is a characteristic length scale that renders the ionic conductivity dependent on the length-scale of the microstructure. This is reminiscent of surface energy effects [49–51] or gradient-type continuum theories [52,53].

The dimensionless form of the governing equations become

$$\bar{\nabla}\cdot(-\epsilon_r\bar{\nabla}\bar{\xi})-\frac{\Phi^2}{\bar{\beta}}(\bar{\mu}-\bar{\tilde{\mu}})+\frac{\bar{\nu}_i}{\bar{\beta}}\frac{\Phi^2}{\Gamma}\bar{\Pi}=0 \tag{37}$$

$$\bar{\nabla}\cdot[\bar{\nabla}\bar{\mathbf{u}}+\mathbf{I}-\det(\bar{\nabla}\bar{\mathbf{u}}+\mathbf{I})\bar{\Pi}(\bar{\nabla}\bar{\mathbf{u}}+\mathbf{I})^{-T}]=0 \tag{38}$$

$$\bar{\nabla}\cdot\left[-\bar{\gamma}\left(\frac{\Gamma}{\bar{\beta}}(\bar{\mu}-\bar{\tilde{\mu}})-\bar{\Pi}\frac{\bar{\nu}_i}{\bar{\beta}}+\bar{c}_0\right)\bar{\nabla}(\bar{\mu}+\bar{\xi})\right]=\frac{H^2}{\mu_{\text{ref}}\gamma_{\text{ref}}}\frac{1}{T}\frac{\mathrm{d}}{\mathrm{d}\bar{t}}\left(\frac{\Gamma}{\bar{\beta}}(\bar{\mu}-\bar{\tilde{\mu}})-\bar{\Pi}\frac{\bar{\nu}_i}{\bar{\beta}}+\bar{c}_0\right) \tag{39}$$

where $\Phi=Hqc_{\text{ref}}/\sqrt{\epsilon_0 G_{\text{ref}}}$ and $\Gamma=\mu_{\text{ref}}c_{\text{ref}}/G_{\text{ref}}$.

3.2 Weak Form. We write the weak forms of governing equations by employing three test functions ν, ω, and ρ for the scalar electric potential ξ, displacement vector $\mathbf{u}$, and the chemical potential μ. By multiplying the governing equations by the test functions, integrating over the volume, and using the divergence theorem, the weak forms can be written as follows:

$$\int_{\partial\Omega}\bar{\nabla}\cdot(-\epsilon_r\bar{\nabla}\bar{\xi})\nu.\mathbf{n}_{\text{i}}\,\mathrm{d}S-\int_\Omega(-\epsilon_r\bar{\nabla}\bar{\xi})\bar{\nabla}\nu\,\mathrm{d}V-\int_\Omega\left(\frac{\Phi^2}{\bar{\beta}}(\bar{\mu}-\bar{\tilde{\mu}})\nu+\frac{\bar{\alpha}_{\text{el}}}{\bar{\beta}}\frac{\Phi^2}{\Gamma}\bar{\nabla}\cdot(\bar{\mathbf{u}})\right)\nu\,\mathrm{d}V=0 \tag{40}$$

$$\int_{\partial\Omega}\left[\frac{\mathbb{C}}{G_{\text{ref}}}\bar{\nabla}\bar{\mathbf{u}}+\bar{\alpha}_{\text{el}}\frac{\Gamma}{\bar{\beta}}(\bar{\mu}-\bar{\tilde{\mu}})\mathbf{I}-\frac{\bar{\alpha}_{\text{el}}{}^2}{\bar{\beta}}\bar{\nabla}\cdot\bar{\mathbf{u}}\mathbf{I}\right]\omega\cdot\mathbf{n}_{\text{i}}\,\mathrm{d}S-\int_\Omega\left[\frac{\mathbb{C}}{G_{\text{ref}}}\bar{\nabla}\bar{\mathbf{u}}+\bar{\alpha}_{\text{el}}\frac{\Gamma}{\bar{\beta}}(\bar{\mu}-\bar{\tilde{\mu}})\mathbf{I}-\frac{\bar{\alpha}_{\text{el}}{}^2}{\bar{\beta}}\bar{\nabla}\cdot\bar{\mathbf{u}}\mathbf{I}\right]\bar{\nabla}\omega\,\mathrm{d}V=0 \tag{41}$$

$$\int_{\partial\Omega}\left[-\bar{\gamma}\left(\frac{\Gamma}{\bar{\beta}}(\bar{\mu}-\bar{\tilde{\mu}})-\bar{\nabla}\cdot\bar{\mathbf{u}}\frac{\bar{\alpha}_{\text{el}}}{\bar{\beta}}+\bar{c}_0\right)\bar{\nabla}(\bar{\mu}+\bar{\xi})\right]\rho\cdot\mathbf{n}_{\text{i}}\,\mathrm{d}S-\int_\Omega\left[-\bar{\gamma}\left(\frac{\Gamma}{\bar{\beta}}(\bar{\mu}-\bar{\tilde{\mu}})-\bar{\nabla}\cdot\bar{\mathbf{u}}\frac{\bar{\alpha}_{\text{el}}}{\bar{\beta}}+\bar{c}_0\right)\bar{\nabla}(\bar{\mu}+\bar{\xi})\right]\bar{\nabla}\cdot\rho\,\mathrm{d}V=\int_\Omega\frac{H^2}{\mu_{\text{ref}}\gamma_{\text{ref}}}\frac{1}{T}\frac{\mathrm{d}}{\mathrm{d}\bar{t}}\left(\frac{\Gamma}{\bar{\beta}}(\bar{\mu}-\bar{\tilde{\mu}})-\bar{\nabla}\cdot\bar{\mathbf{u}}\frac{\bar{\alpha}_{\text{el}}}{\bar{\beta}}+\bar{c}_0\right)\rho\,\mathrm{d}V \tag{42}$$

Test functions ω, ν, and ρ on the boundary are constrained to be zero.

$$\omega=\rho=\nu=0\quad\text{on }\partial\Omega \tag{43}$$

Using Eq. (43) the first terms of Eqs. (40), (41), (42) are equal to zero, as follows,

$$\int_{\partial\Omega}\nabla\cdot(-\epsilon_r\nabla\bar{\xi})\nu\cdot\mathbf{n}_{\text{i}}\,\mathrm{d}S=0 \tag{44}$$

$$\int_{\partial\Omega}\left[\frac{\mathbb{C}}{G_{\text{ref}}}\bar{\nabla}\bar{\mathbf{u}}+\bar{\alpha}_{\text{el}}\frac{\Gamma}{\bar{\beta}}(\bar{\mu}-\bar{\tilde{\mu}})\mathbf{I}-\frac{\bar{\alpha}_{\text{el}}{}^2}{\bar{\beta}}\nabla\cdot\bar{\mathbf{u}}\mathbf{I}\right]\omega\cdot\mathbf{n}_{\text{i}}\,\mathrm{d}S=0 \tag{45}$$

$$\int_{\partial\Omega}\left[-\bar{\gamma}\left(\frac{\Gamma}{\bar{\beta}}(\bar{\mu}-\bar{\tilde{\mu}})-\bar{\nabla}\cdot\bar{\mathbf{u}}\frac{\bar{\alpha}_{\text{el}}}{\bar{\beta}}+\bar{c}_0\right)\bar{\nabla}(\bar{\mu}+\bar{\xi})\right]\rho\cdot\mathbf{n}_{\text{i}}\,\mathrm{d}S=0 \tag{46}$$

Using Eqs. (44), (45), and (46), Eqs. (40), (41), and (42) will be shorten to the following forms,

$$-\int_\Omega(-\epsilon_r\bar{\nabla}\bar{\xi})\bar{\nabla}\nu\,\mathrm{d}V-\int_\Omega\left(\frac{\Phi^2}{\bar{\beta}}(\bar{\mu}-\bar{\tilde{\mu}})\nu+\frac{\bar{\alpha}_{\text{el}}}{\bar{\beta}}\frac{\Phi^2}{\Gamma}\bar{\nabla}\cdot(\bar{\mathbf{u}})\right)\nu\,\mathrm{d}V=0 \tag{47}$$

$$\int_\Omega\left[\frac{\mathbb{C}}{G_{\text{ref}}}\bar{\nabla}\bar{\mathbf{u}}+\bar{\alpha}_{\text{el}}\frac{\Gamma}{\bar{\beta}}(\bar{\mu}-\bar{\tilde{\mu}})\mathbf{I}-\frac{\bar{\alpha}_{\text{el}}{}^2}{\bar{\beta}}\bar{\nabla}\cdot\bar{\mathbf{u}}\mathbf{I}\right]\bar{\nabla}\omega\,\mathrm{d}V=0 \tag{48}$$

$$-\int_\Omega\left[-\bar{\gamma}\left(\frac{\Gamma}{\bar{\beta}}(\bar{\mu}-\bar{\tilde{\mu}})-\bar{\nabla}\cdot\bar{\mathbf{u}}\frac{\bar{\alpha}_{\text{el}}}{\bar{\beta}}+\bar{c}_0\right)\bar{\nabla}(\bar{\mu}+\bar{\xi})\right]\bar{\nabla}\cdot\rho\,\mathrm{d}V=\int_\Omega\frac{H^2}{\mu_{\text{ref}}\gamma_{\text{ref}}}\frac{1}{T}\frac{\mathrm{d}}{\mathrm{d}\bar{t}}\left(\frac{\Gamma}{\bar{\beta}}(\bar{\mu}-\bar{\tilde{\mu}})-\bar{\nabla}\cdot\bar{\mathbf{u}}\frac{\bar{\alpha}_{\text{el}}}{\bar{\beta}}+\bar{c}_0\right)\rho\,\mathrm{d}V \tag{49}$$

For the system in Eq. (25), the weak form can be written as follows:

$$-\int_\Omega(-\epsilon_r\bar{\nabla}\bar{\xi})\bar{\nabla}\nu\,\mathrm{d}V-\int_\Omega\left(\frac{\Phi^2}{\bar{\beta}}(\bar{\mu}-\bar{\tilde{\mu}})\nu+\frac{\bar{\nu}_i}{\bar{\beta}}\frac{\Phi^2}{\Gamma}\bar{\Pi}\right)\nu\,\mathrm{d}V=0 \tag{50}$$

$$\int_\Omega\left[\bar{\nabla}\bar{\mathbf{u}}+\mathbf{I}-\det(\bar{\nabla}\bar{\mathbf{u}}+\mathbf{I})\bar{\Pi}(\bar{\nabla}\bar{\mathbf{u}}+\mathbf{I})^{-T}\right]\bar{\nabla}\omega\,\mathrm{d}V=0 \tag{51}$$

$$-\int_\Omega\left[-\bar{\gamma}\left(\frac{\Gamma}{\bar{\beta}}(\bar{\mu}-\bar{\tilde{\mu}})-\bar{\Pi}\frac{\bar{\nu}_i}{\bar{\beta}}+\bar{c}_0\right)\bar{\nabla}(\bar{\mu}+\bar{\xi})\right]\bar{\nabla}\cdot\rho\,\mathrm{d}V=\int_\Omega\frac{H^2}{\mu_{\text{ref}}\gamma_{\text{ref}}}\frac{1}{T}\frac{\mathrm{d}}{\mathrm{d}\bar{t}}\left(\frac{\Gamma}{\bar{\beta}}(\bar{\mu}-\bar{\tilde{\mu}})-\bar{\Pi}\frac{\bar{\nu}_i}{\bar{\beta}}+\bar{c}_0\right)\rho\,\mathrm{d}V \tag{52}$$

3.3 Implementation in *FEniCS*. The governing equations presented in the previous section (in their weak form) are solved using the general-purpose open-source PDE solver *FEniCS*. The weak forms and the corresponding finite element discretization are specified using a domain-specific language, named UFL (Unified Form Language) embedded in PYTHON. The computational domain is partitioned into non-overlapping triangular elements with quadratic interpolation for displacement and linear interpolation for chemical and electric potential in a continuous Galerkin function space. The discrete trial and test spaces are defined by constructing finite element shape functions over the union of all elements in Ω [54].

4 Benchmark Solutions

Before proceeding to analyze microstructures that are intractable analytically, to ensure first that our finite element implementation is correct, we compare our numerical calculations with some known analytical results.

4.1 Uniform Electrolyte. We first analyze the the simplified problem of a one-dimensional and homogeneous electrolyte as shown in the Fig. 3 with electric potential difference between two charge collectors $\Delta\xi=(\xi_1-\xi_0)$. Elasticity is decoupled for this illustrative problem so we set $\alpha=0$. The analytical result for the chemical potential along the thickness of the electrolyte is given by

$$\mu(x)=\frac{\mu_0-\eta\mu_d}{1-\eta^2}e^{-(x/\lambda)}+\frac{-\eta\mu_0+\mu_d}{1-\eta^2}e^{(x-d)/\lambda} \tag{53}$$

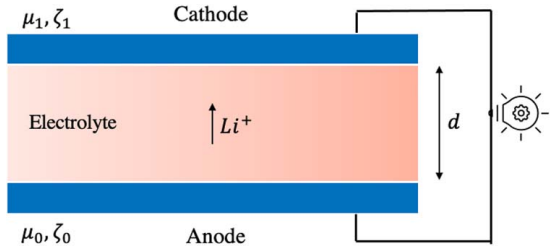

Fig. 3 Schematic of a system of uniform electrolyte and electrodes in a battery

where λ_r is the Debye length and $\eta = e^{-(d/\lambda_r)}$ [34]. In Fig. 4, we contrast the results of our finite element calculation with the closed-form solution.

4.2 Multi-Layer Composite Solid Electrolyte. As partially discussed the context of Fig. 1, past research appears to indicate that addition of nano-particles in a polymer alters the region in the vicinity of the particle thus forming an interphase layer. The interphase layer, while substantively the same as the polymer matrix in physical and mechanical behavior, exhibits significantly higher ionic mobility than the polymer [55]. In short, a three-phase composite consisting of an inclusion (typically ceramic), its surrounding matrix (typically soft polymer) and an interphase region, is an adequate description of actual solid composite electrolyte systems. We note that [45] also utilizes this observation. Arguably, the simplest possible composite electrolyte is a multi-layer laminate. The problem essentially becomes one-dimensional in nature. In this section, we benchmark our numerical results for a three-layer solid electrolyte laminate structure (Fig. 5).

Denoting the total thickness of the system by d, we refer to the inclusion, polymer and interphase dimensions as d_p, d_{int}, and d_f, respectively. We define a constant of proportionality, α, called interphase extension factor, to introduce the normalization of d_{int} with respect to the size of the inclusion as follows:

$$d_{int} = \alpha d_f = \alpha \nu_f d \tag{54}$$

To generate numerical results and study the effect of volume fraction, we fix the inclusion size to a thickness of 2 nm and vary the thickness of the polymer (d_p). The calculations are performed for different interphase extension factors. We note that the results are *size-dependent* unlike classical conductivity problems.

Figure 6 shows the normalized effective ionic conductivity with respect to the volume fraction of the filler $\nu_f = d_f/d$ for different values of α. We remark that K_0 is the ionic conductivity of the case when $\nu_f = 0$. The $\alpha = 0$ corresponds to an absence of an interphase and, as expected, the effective ionic conductivity of the composite does not vary much with an increase in volume fraction of the inclusion phase. However, when $\alpha > 0$, we see a significant enhancement. This is hardly surprising since the interphase region has been found to be highly conductive and larger this phase, higher the effective ionic conductivity. This corresponds well with the thesis (and experimental observation) that even though second-phase particles may not be by themselves ionically conductive, they alter the region around the particles to make it more conductive.

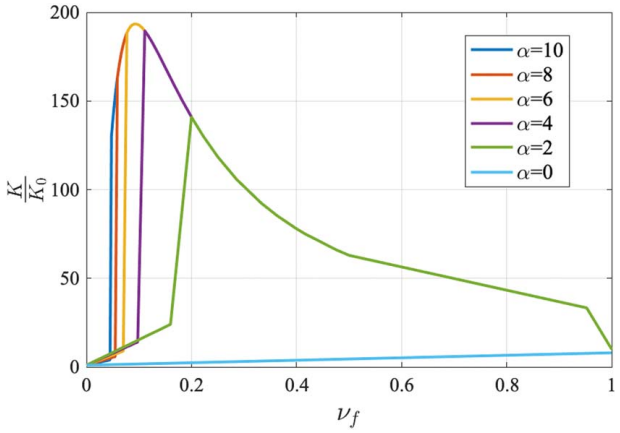

Fig. 6 Normalized effective ionic conductivity with respect to the volume fraction of the inclusion phase. $\gamma^{\text{filler}} = \gamma^{\text{polymer}} = \gamma^{\text{interphase}}/1000$ the initial concentration is considered as zero ($c_0^{\text{filler}} = 0$) and for interphase and polymer we have $c_0^{\text{interphase}} = c_0^{\text{polymer}} = 50\ \frac{\text{mol}}{\text{m}^3}$. The numerical values are $\lambda_r^{\text{interphase}} = \lambda_r^{\text{filler}} = \lambda_r^{\text{polymer}} = 4$ nm, $\epsilon_r^{\text{filler}} = 10$, $\epsilon_r^{\text{polymer}} = \epsilon_r^{\text{interphase}} = 3$, $\hat{\mu}^{\text{polymer}} = \hat{\mu}^{\text{interphase}} = 0.5$ eV, and $\hat{\mu}^{\text{polymer}} - \hat{\mu}^{\text{filler}} = 1$ eV.

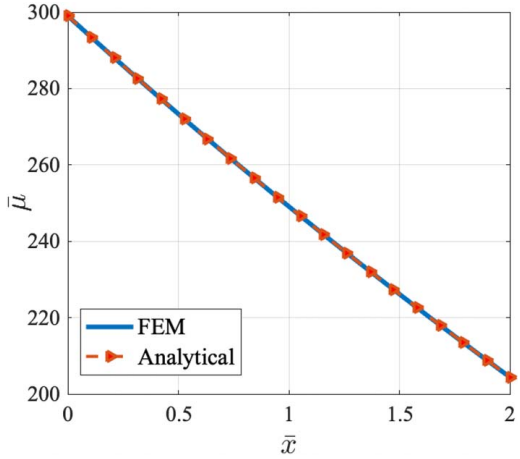

Fig. 4 Normalized chemical potential across the normalized thickness of rectangular uniform unit cell material

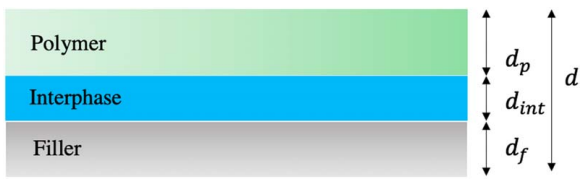

Fig. 5 Schematic of a multi-layer composite electrolyte consisting of a filler, an interphase, and polymer

5 Heterogeneous Electrolytes With Ellipsoidal Inclusions—Shape Effects

We now turn to one of the central results of our paper where we analyze a microstructure that is not amenable to analytical solution—ellipsoidal inclusions.The ellipsoidal shape allows us to study the effect of particle shape on the effective conductivity enhancement. We remark that this specific insight does not appear to have been discussed in the literature so far.

As shown in Fig. 7, we consider the two-dimensional case of an elliptical inclusion with the major and minor axes, $2b$ and $2a$ in a square unit cell of polymer matrix (of length L). The interphase of thickness t is assumed to be uniform and we will analyze the steady-state limit of the governing equations.

In what follows, we fix the interphase thickness (t) and vary the interphase extension factor (α) which can be defined as $\alpha = t/a$. We first analyze the simplified case of circular geometry ($a = b$). We remark that the case of a single circular inclusion case can indeed be solved analytically (c.f. Ref. [34]); however, homogenization can only proceed approximately. Of course, in the case of a general elliptical inclusion neither the problem of a single inclusion nor the homogenization are analytically tractable. For the circular inclusion case study, we fix the size of the particle ($a = b = 1$ nm) and volume fraction is altered by varying L. The unit cell is subject to a constant electric potential difference $\Delta\mu = 200 \times \mu_{\text{ref}} = 100$eV. In equilibrium situation ($\phi = 0$), the $\Delta\xi = -(\Delta\mu/q) = -100$ V.

Figure 8 illustrates the normalized effective ionic conductivity versus volume fraction of an embedded circular filler in a square unite cell. Here, K_0 represents the ionic conductivity of a uniform polymer electrolyte. We observe essentially the same trend as in

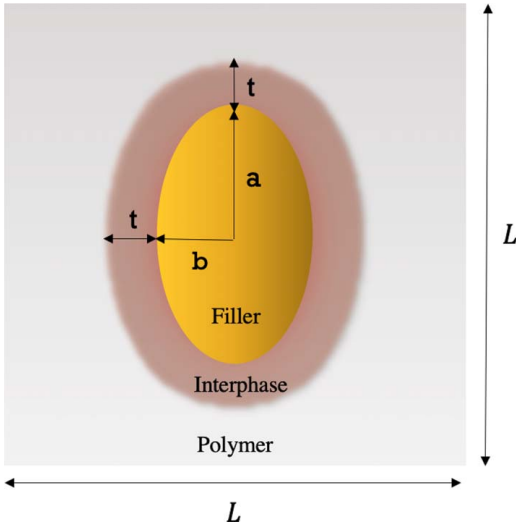

Fig. 7 Schematic of an embedded elliptical inclusion

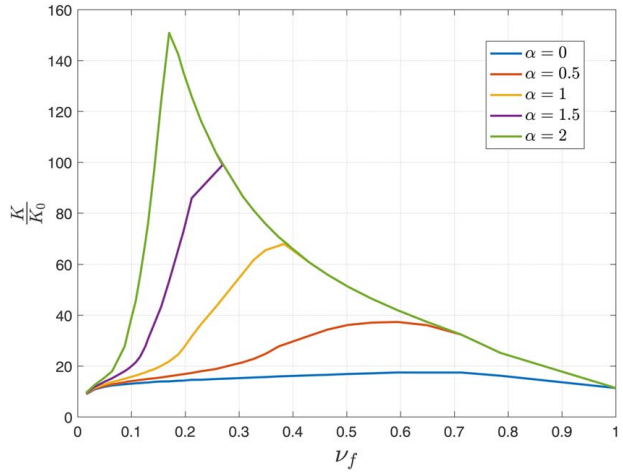

Fig. 8 Normalized ionic conductivity with respect to the volume fraction of the filler for different interphase extension factors (α). $\gamma^{filler} = \gamma^{polymer} = \gamma^{interphase}/1000$ the initial concentration is considered as zero ($c_0^{filler} = 0$) and for interphase and polymer we have $c_0^{interphase} = c_0^{polymer} = 50\,\frac{mol}{m^3}$. The numerical values are $\lambda_r^{interphase} = \lambda_r^{filler} = \lambda_r^{polymer} = 4\,nm$, $\epsilon_r^{filler} = 10, \epsilon_r^{polymer} = \epsilon_r^{interphase} = 3$, $\hat{\mu}^{polymer} = \hat{\mu}^{interphase} = 0.5\,eV$, and $\hat{\mu}^{polymer} - \hat{\mu}^{filler} = 1\,eV$

Fig. 6 where the effective ionic conductivity of the composite reaches a maximum point (for some specific volume fraction) and then decreases to its initial value. Consistent with the one-dimensional study in the preceding section, the interphase plays a dominant role and (as example), for $\alpha = 2$, we see that the ionic conductivity enhances by an order of magnitude. For any $\alpha > 0$, the composite reaches its maximum effective ionic conductivity at the point where the interphase reaches it's maximum volume fraction in a unit cell.

To better illustrate this phenomenon, we show in Fig. 9, a square unit cell with an embedded circular filler with $\alpha = 1$ for three different values for volume fractions 0.78, 0.43, and 0.12. Each of these three figures shows an individual point on the graph in Fig. 8 where $\alpha = 1$. Evidently, the maximum effective ionic conductivity occurs when the interphase content is maximized.

Figures 10–12 illustrate the chemical potential, electric potential, and concentration contours, respectively, for all three different values of volume fraction of the filler, 0.78, 0.43, and 0.12 from

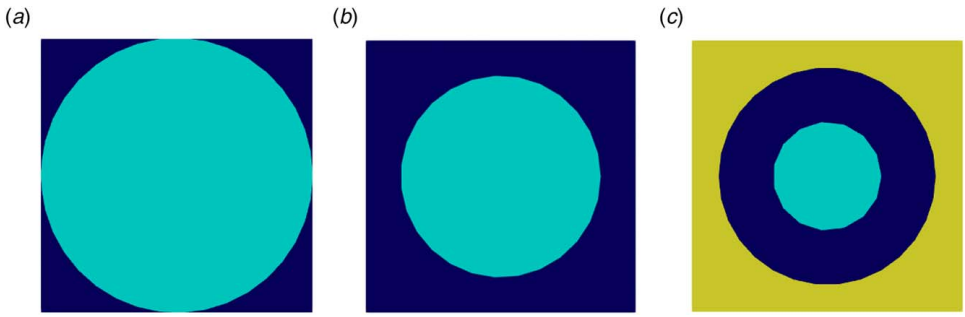

Fig. 9 Schematic of a square unit cell matrix with an embedded circular filler inclusion for $\alpha = 1$ with different values for volume fraction: (a) $\nu_f = 0.78$, (b) $\nu_f = 0.43$, and (c) $\nu_f = 0.12$ where the inclusion (light blue), coating (dark blue), and matrix (yellow) represent the filler, interphase, and polymer, respectively

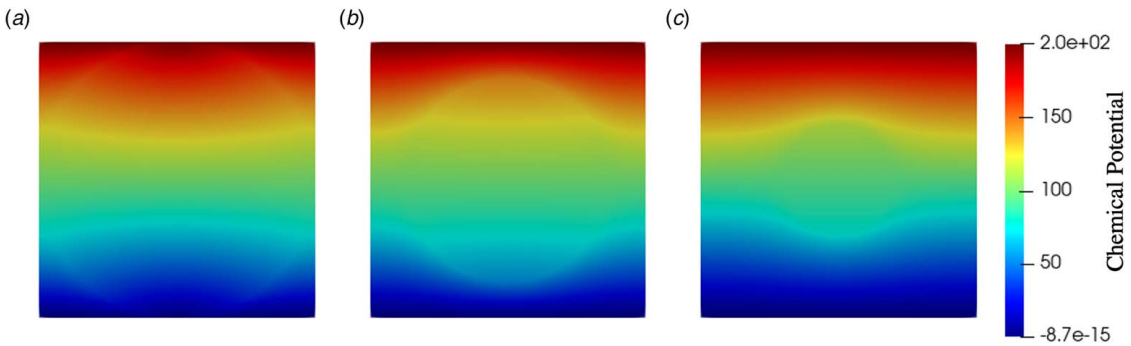

Fig. 10 Chemical potential contour for a square unit cell matrix with an embedded circular filler inclusion for $\alpha = 1$ with different values for volume fraction: (a) $\nu_f = 0.78$, (b) $\nu_f = 0.43$, and (c) $\nu_f = 0.12$

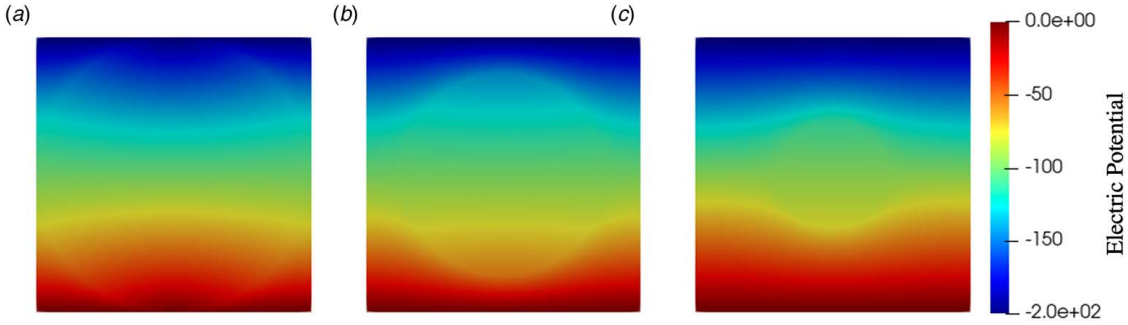

Fig. 11 Electric potential contour for a square unit cell matrix with an embedded circular filler inclusion for $\alpha = 1$ with different values for volume fraction: (a) $v_f = 0.78$, (b) $v_f = 0.43$, and (c) $v_f = 0.12$

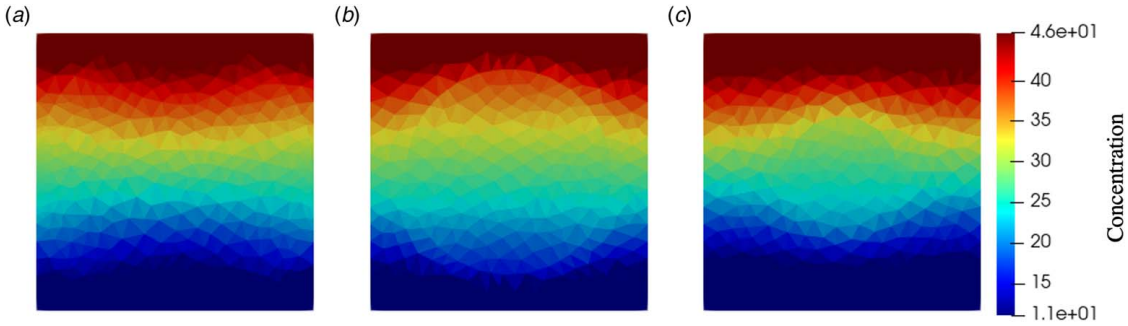

Fig. 12 Concentration contour for a square unit cell matrix with an embedded circular filler inclusion for $\alpha = 1$ with different values for volume fraction: (a) $v_f = 0.78$ (b) $v_f = 0.43$, and (c) $v_f = 0.12$

(*a*) to (*c*), respectively, under the same boundary conditions for the unit cell in equilibrium situation ($\phi = 0$), where $\Delta\mu = 200 \times \mu_{\text{ref}} = 100$ eV and $\Delta\xi = -(\Delta\mu/q) = -100$ V. In a battery-like system, the electrolyte is subjected to a potential difference from the electrodes(anode and cathode), therefore as a result we can see in Fig. 12 that the concentration in all three situations reaches its maximum value, 4.6, at the point where the chemical potential is at its maximum value on the top boundary. Also, the minimum concentration is reported exactly at the point we have the minimum chemical potential on the bottom boundary. Therefore, the difference in effective conductivity in all these three situations is not a result of the difference in maximum and minimum value of concentration, but rather,

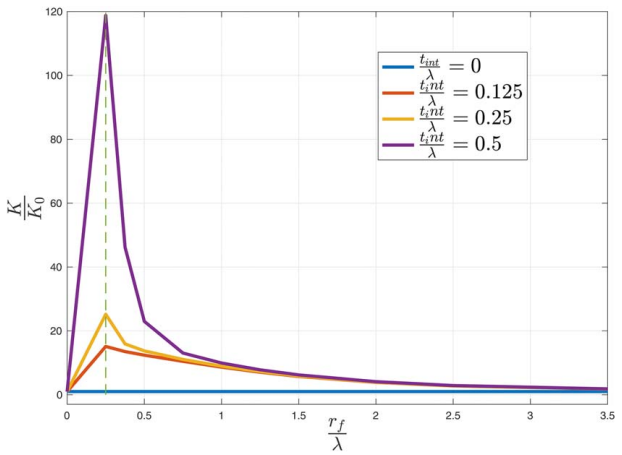

Fig. 13 Normalized ionic conductivity with respect to the normalized radius of the circular inclusion with a constant volume fraction of the filler ($v_f = 0.2$) for different interphase thickness (t_{int}) from 0 to 2 nm which is normalized with debye length ($\lambda_r =$ 4 nm). $\gamma^{filler} = \gamma^{polymer} = \gamma^{interphase}/1000$ the initial concentration is considered as zero ($c_0^{filler} = 0$) and for interphase and polymer we have $c_0^{interphase} = c_0^{polymer} = 50\,\frac{\text{mol}}{\text{m}^3}$. The numerical values are $\lambda_r^{interphase} = \lambda_r^{filler} = \lambda_r^{polymer} = 4$ nm, $\epsilon_r^{filler} = 10$, $\epsilon_r^{polymer} = \epsilon_r^{interphase} = 3$, $\hat{\mu}^{\text{polymer}} = \hat{\mu}^{\text{interphase}} = 0.5$ eV, and $\hat{\mu}^{\text{polymer}} - \hat{\mu}^{\text{filler}} = 1$ eV.

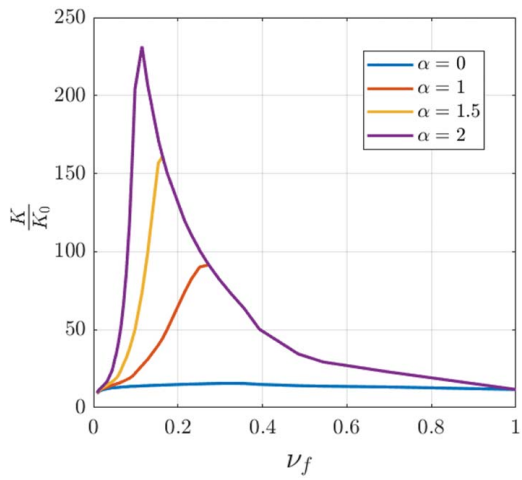

Fig. 14 Normalized ionic conductivity with respect to the volume fraction of the elliptical filler for different interphase extension factors (α) $\gamma^{filler} = \gamma^{polymer} = \gamma^{interphase}/1000$ the initial concentration is considered as zero ($c_0^{filler} = 0$) and for interphase and polymer we have $c_0^{interphase} = c_0^{polymer} = 50\,\frac{\text{mol}}{\text{m}^3}$. The numerical values are $\lambda_r^{interphase} = \lambda_r^{filler} = \lambda_r^{polymer} = 4$ nm, $\epsilon_r^{filler} = 10$, $\epsilon_r^{polymer} = \epsilon_r^{interphase} = 3$, $\hat{\mu}^{\text{polymer}} = \hat{\mu}^{\text{interphase}} = 0.5$ eV, and $\hat{\mu}^{\text{polymer}} - \hat{\mu}^{\text{filler}} = 1$ eV.

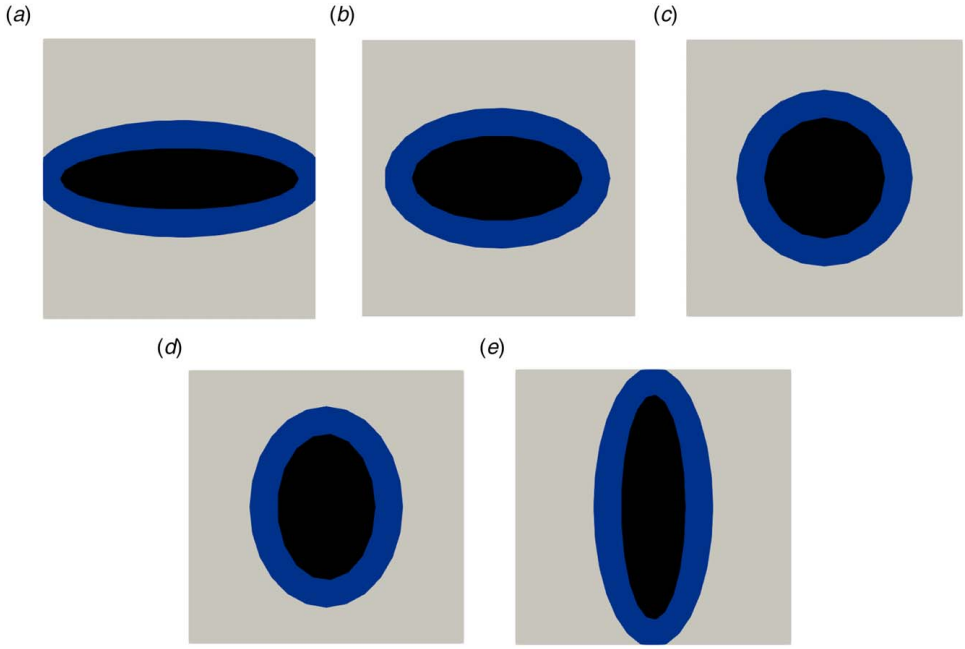

Fig. 15 Schematics of a square unit cell matrix with an embedded elliptical inclusion with interphase thickness of $t_{int} = 1$ nm with different *a*/*b*: (*a*) 0.25, (*b*) 0.5, (c) 1, (*d*) 1.5, and (*e*) 3.5

it is due to the concentration distribution and the difference in ion mobility of within each layer.

Since we now have insight into the filler volume fraction at which the maximum ionic conductivity in a composite electrolyte is achieved, we can examine the effect of inclusion size. To that end, we assume a constant volume fraction of filler ($\nu_f = 0.2$) and vary the radius of the inclusion from 1 nm to 14 nm for four different interphase extension factors. Figure 13 illustrates the ionic conductivity of the composite with respect to the radius of the inclusion. For a given volume fraction, there is an optimal size and thus our model correctly resolves experimental observations that both an increase and decrease in ionic conductivity can occur with addition of fillers—the tuning of volume fraction and size is an important element to decide what behavior will be observed. We remark that for large inclusion size, we approach the matrix ionic conductivity ($K/K_0 = 1$).

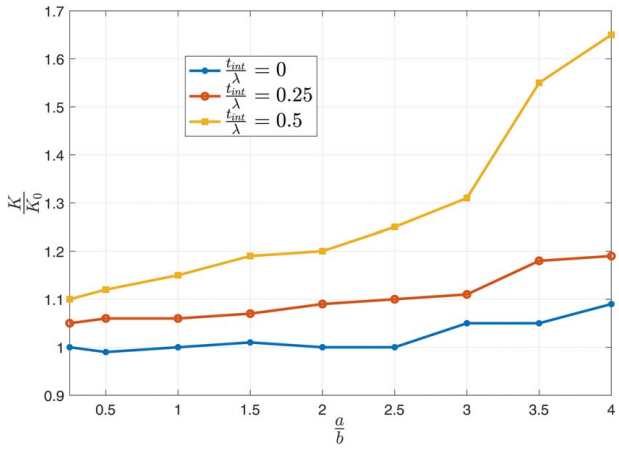

Fig. 16 Normalized ionic conductivity with respect to *a*/*b* for different interphase thickness from 0 to 2 nm which is normalized by Debye length ($\lambda = 4$ nm). The ionic conductivity is normalized with the case of the $\alpha = 0$ and $a/b = 0.2$. The detailed numerical values are adapted from Fig. 12 caption.

We now turn to elliptical shaped fillers where $a = 1$ nm, $b = 0.5$ nm in Fig. 14. We note a similar trend as in Fig. 8.

Comparing Figs. 14 and 8, we see that the maximum for elliptical fillers is higher compared to circular counterparts. This prompts a closer examination of the role of ellipse aspect ratio. For that, we consider a square unit cell matrix with fixed $L = 10$ nm and elliptical inclusions with lengths a and b with interphase expansion factor of α.

Figure 15 illustrates five different case with different value of *a*/*b* for $t_{int} = 1$ in (*a*), (*b*), (*c*), (*d*), and (*e*) which represent five cases in a range of *a*/*b* from 0 + up to 4.

Figure 16 illustrates the normalized ionic conductivity of the square unit cell matrix with an embedded elliptical filler with respect to the ratio *a*/*b* of the elliptical filler for three different values of α and otherwise the same boundary conditions. We can conclude that as *a*/*b* increases, the effective ionic conductivity of the composite is enhanced. Also, as the interphase thickness (t_{int}) increases, the effect of *a*/*b* becomes more pronounced.

6 Effect of Deformation on the Ionic Conductivity of an Electrolyte

In the preceding sections, for simplicity and to facilitate insights, we had neglected the coupling between elasticity and electrodiffusion. In this section, for studying the effect of deformation on ionic conductivity of an electrolyte, we consider the full time-dependent fully coupled electro-elasto-chemical system of equations and also attempt to ascertain the impact of considering nonlinear deformation. We consider the configuration in Fig. 17, where an electrolyte is assumed to be stretched from two ends.

To study the effect of deformation on composite electrolytes, we consider a multi-layered system as previously shown in Fig. 5.

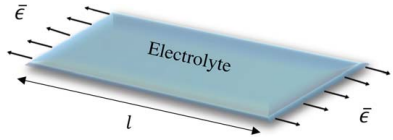

Fig. 17 Schematic of a unit cell under a stretch of ϵ

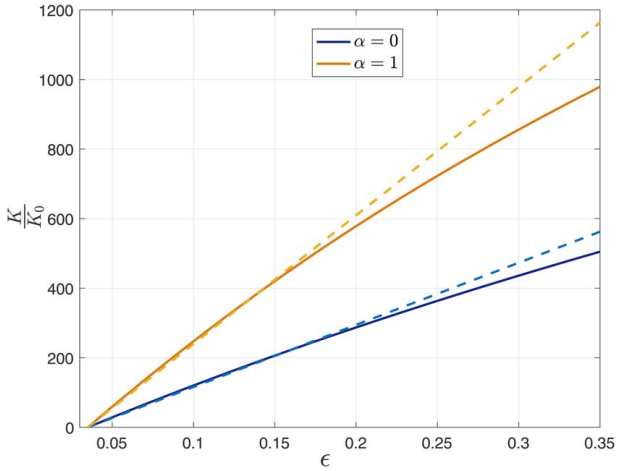

Fig. 18 Normalized ionic conductivity versus average strain for different interphase extension factors α. The dashed lines are the case of small deformation and the solid lines are for the case of elastically incompressible model. The ionic conductivity is normalized with the case of the homogeneous system. The detailed numerical values are adapted from Fig. 13 caption. Also, $v_i = 1.8 \times 10^{-28}$ m^3, $v_f = 0.3$, $\alpha_{el} = 10^{-6} \times [80,3,3]$ and $Ey = [70,0.03, 0.03]$ GPa.

Figure 18 illustrates the normalized ionic conductivity of a multilayer composite electrolyte with respect to the applied strain for two different extension factors. The dashed lines show the case for small deformation while the solid lines are for the neo-Hookean elastically incompressible model. Clearly, deformation can significantly enhance ionic conductivity. The small deformation model predicts a linear relation between ionic conductivity and strain—also reported in experiments [33]. While there is a departure from this linear relation at large strains, the deviation is perhaps not that high. We would, however, like to state that the polymer system examined in this work is not *too* soft. For softer materials (like gels) nonlinear deformation effects are likely to be more significant.

7 A Proposal for a Microstructure to Enhance Ionic Conductivity: Columnar Dielectric Spacers

In this section, based on the insights at hand, we propose a novel microstructure that simply involves the addition of columnar dielectric spacer in parallel with the electrolyte—as shown in Fig. 19. The key idea is that when we set columnar spacers parallel to the electrolyte, the effective ionic resistance of the composite decreases to a smaller value.

The governing equation for the electrostatics problem is as follows:

$$\begin{cases} -\lambda^2 \nabla^2 \xi + \xi = \frac{\phi}{q} & \text{in electrolyte} \\ \nabla^2 \xi = 0 & \text{in dielectrics} \end{cases} \tag{55}$$

The interfacial condition across the electrolyte-dielectric interfaces should be

$$[[\xi]] = 0, \quad [[\epsilon \nabla \xi]] \cdot n = 0 \tag{56}$$

Physically, the interfacial conditions imply that there is no accumulation of free charges at the interface, though the free charge density (per unit volume) may be nonzero in the electrolyte. Though the general solution to Eq. (55) and (56) may be complicated, from linearity, we observe that the electric potential difference should depend on $\Delta\phi$ linearly:

$$\Delta\xi = \alpha_1 \Delta\phi + \alpha_0 \tag{57}$$

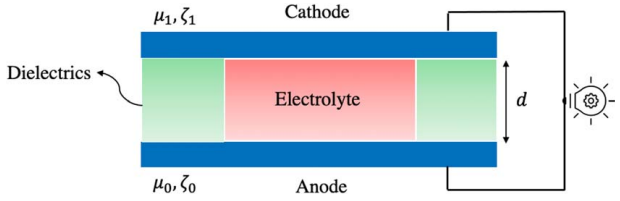

Fig. 19 Schematic of a battery with an electrolyte and columnar dielectric spacers

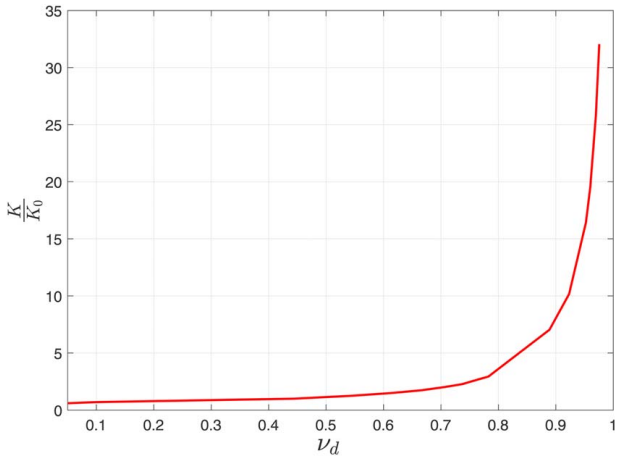

Fig. 20 Normalized ionic conductivity with respect to the volume fraction of dielectric. $\gamma^{\text{dielectric}}/\gamma^{\text{electrolyte}} \approx 0$ the initial ionic concentration of the dielectric is considered as zero ($c_0^{\text{dielectric}} = 0$) while for electrolyte we have $c_0^{\text{electrolyte}} = 100 \frac{\text{mol}}{\text{m}^3}$

Figure 20 illustrates the normalized effective ionic conductivity with respect to volume fraction of the columnar spacers. In this model, the size of the electrolyte is constant and the size of the dielectric increases from zero to a large number to ensure that the range of volume fraction is from 0 to 1. The graph shows enhancement in the ionic conductivity of the composite electrolyte by the addition of dielectric columnar spacers, and more importantly, increase in the size of the spacers further improves the enhancement of ionic conductivity. We remark that for this microstructure, the effective ionic conductivity can potentially increase by an order of magnitude. The addition of the dielectric spacers in parallel with the electrolyte also helps enhance the electric field in the electrolyte which facilitates ionic conduction. The compelling feature related to this microstructure is that it is very easy to fabricate. However, we do caution that the significant enhancement does appear to be at very high volume fractions which may not be very practical.

8 Concluding Remarks

In this paper, we have presented a numerical implementation of the governing equations that dictate the electro-chemo-mechanical behavior of soft deformable solid electrolytes within an open-source finite element package *FEniCS*. The implementation is validated with known analytical solutions for some simplified cases. The numerical implementation allows us to design complex microstructures for the enhancement of ionic conductivity of solid electrolytes. Specifically, we were able to obtain insights into how the shape of embedded particles can influence the overall ionic conductivity of a composite electrolyte in addition to proposing a new type of microstructure to achieve this objective. A good future direction would be the use of topology optimization tools (including machine learning) to find optimal microstructures. With composite electrolytes, such

as those discussed in this paper, durability of the chemo-mechanical-electrical system under cyclic loading such as discussed in other contexts also [56] is likely to become a significant issue.

Acknowledgment

We gratefully acknowledge partial support from the M.D. Anderson Professorship.

Conflict of Interest

There are no conflicts of interest.

Data Availability Statement

The authors attest that all data for this study are included in the paper.

References

[1] Chu, S., and Majumdar, A., 2012, "Opportunities and Challenges for a Sustainable Energy Future," Nature, **488**(7411), pp. 294–303.
[2] Zito, R., and Ardebili, H., 2019, *Energy Storage: A New Approach*, 2nd ed., Wiley-Scrivener, Beverly, MA.
[3] Kasavajjula, U., Wang, C., and Appleby, A. J., 2007, "Nano-and Bulk-Silicon-Based Insertion Anodes for Lithium-Ion Secondary Cells," J. Power Sources, **163**(2), pp. 1003–1039.
[4] Prosini, P. P., Lisi, M., Zane, D., and Pasquali, M., 2002, "Determination of the Chemical Diffusion Coefficient of Lithium in Lifepo4," Solid State Ionics, **148**(1–2), pp. 45–51.
[5] Goodenough, J. B., and Park, K.-S., 2013, "The Li-Ion Rechargeable Battery: A Perspective," J. Am. Chem. Soc., **135**(4), pp. 1167–1176.
[6] Winter, M., and Besenhard, J. O., 1999, "Electrochemical Lithiation of Tin and Tin-Based Intermetallics and Composites," Electrochim. Acta, **45**(1–2), pp. 31–50.
[7] Lukatskaya, M. R., Dunn, B., and Gogotsi, Y., 2016, "Multidimensional Materials and Device Architectures for Future Hybrid Energy Storage," Nat. Commun., **7**(1), pp. 1–13.
[8] Xu, K., 2014, "Electrolytes and Interphases in Li-Ion Batteries and Beyond," Chem. Rev., **114**(23), pp. 11503–11618.
[9] Kumar, S. A., and Kuppusami, P., 2020, "Enhancing the Ionic Conductivity in the Ceria-Based Electrolytes for Intermediate Temperature Solid Oxide Fuel Cells," *Intermediate Temperature Solid Oxide Fuel Cells*, Elsevier, pp. 113–163.
[10] Xu, K., 2004, "Nonaqueous Liquid Electrolytes for Lithium-Based Rechargeable Batteries," Chem. Rev., **104**(10), pp. 4303–4418.
[11] Zhang, H., Li, C., Piszcz, M., Coya, E., Rojo, T., Rodriguez-Martinez, L. M., Armand, M., and Zhou, Z., 2017, "Single Lithium-Ion Conducting Solid Polymer Electrolytes: Advances and Perspectives," Chem. Soc. Rev., **46**(3), pp. 797–815.
[12] Kim, H., Jeong, G., Kim, Y.-U., Kim, J.-H., Park, C.-M., and Sohn, H.-J., 2013, "Metallic Anodes for Next Generation Secondary Batteries," Chem. Soc. Rev., **42**(23), pp. 9011–9034.
[13] Aurbach, D., Zinigrad, E., Cohen, Y., and Teller, H., 2002, "A Short Review of Failure Mechanisms of Lithium Metal and Lithiated Graphite Anodes in Liquid Electrolyte Solutions," Solid State Ionics, **148**(3–4), pp. 405–416.
[14] Tan, S.-J., Zeng, X.-X., Ma, Q., Wu, X.-W., and Guo, Y.-G., 2018, "Recent Advancements in Polymer-Based Composite Electrolytes for Rechargeable Lithium Batteries," Electrochem. Energy Rev., **1**(2), pp. 113–138.
[15] Xu, S., Zhang, Y., Cho, J., Lee, J., Huang, X., Jia, L., and Fan, J. A., et al., 2013, "Stretchable Batteries with Self-Similar Serpentine Interconnects and Integrated Wireless Recharging Systems," Nat. Commun., **4**(1), pp. 1–8.
[16] Kammoun, M., Berg, S., and Ardebili, H., 2016, "Stretchable Spiral Thin-Film Battery Capable of Out-of-Plane Deformation," J. Power Sources, **332**, pp. 406–412.
[17] Ghadi, B. M., Yuan, M., and Ardebili, H., 2019, "Stretchable Fabric-Based Licoo2, Electrode for Lithium Ion Batteries," Extreme Mech. Lett., **32**(7), p. 100532.
[18] Ardebili, H., 2020, "A Perspective on the Mechanics Issues in Soft Solid Electrolytes and the Development of Next-generation Batteries," ASME J. Appl. Mech., **87**(4), p. 040801.
[19] Tang, C., Hackenberg, K., Fu, Q., Ajayan, P. M., and Ardebili, H., 2012, "High Ion Conducting Polymer Nanocomposite Electrolytes Using Hybrid Nanofillers," Nano Lett., **12**(3), pp. 1152–1156.
[20] Li, Q., Wood, E., and Ardebili, H., 2013, "Elucidating the Mechanisms of Ion Conductivity Enhancement in Polymer Nanocomposite Electrolytes for Lithium Ion Batteries," Appl. Phys. Lett., **102**(24), p. 243903.
[21] MacGlashan, G. S., Andreev, Y. G., and Bruce, P. G., 1999, "Structure of the Polymer Electrolyte Poly (ethylene Oxide) 6: Liasf 6," Nature, **398**(6730), pp. 792–794.
[22] Johan, M. R., Shy, O. H., Ibrahim, S., Yassin, S. M. M., and Hui, T. Y., 2011, "Effects of Al2O3 Nanofiller and Ec Plasticizer on the Ionic Conductivity Enhancement of Solid PEO-LiCF3SO3 Solid Polymer Electrolyte," Solid State Ionics, **196**(1), pp. 41–47.
[23] Hirankumar, G., and Mehta, N., 2018, "Effect of Incorporation of Different Plasticizers on Structural and Ion Transport Properties of PVA-LiClO4 Based Electrolytes," Heliyon, **4**(12), p. e00992.
[24] Upadhyay, A. K., and Reddy, C. C., 2017, "On the Mechanism of Charge Transport in Low Density Polyethylene," J. Appl. Phys., **122**(6), p. 064105.
[25] Zhang, S., Li, Z., Guo, Y., Cai, L., Manikandan, P., Zhao, K., Li, Y., and Pol, V. G., 2020, "Room-Temperature, High-Voltage Solid-State Lithium Battery with Composite Solid Polymer Electrolyte With In-Situ Thermal Safety Study," Chem. Eng. J., **400**, p. 125996.
[26] Liu, W., Liu, N., Sun, J., Hsu, P.-C., Li, Y., Lee, H.-W., and Cui, Y., 2015, "Ionic Conductivity Enhancement of Polymer Electrolytes With Ceramic Nanowire Fillers," Nano Lett., **15**(4), pp. 2740–2745.
[27] Wang, Y.-J., Pan, Y., and Kim, D., 2006, "Conductivity Studies on Ceramic Li1. 3Al0. 3Ti1. 7 (PO4) 3-Filled Peo-Based Solid Composite Polymer Electrolytes," J. Power Sources, **159**(1), pp. 690–701.
[28] Croce, F., Appetecchi, G. B., Persi, L., and Scrosati, B., 1998, "Nanocomposite Polymer Electrolytes for Lithium Batteries," Nature, **394**(6692), pp. 456–458.
[29] Weston, J. E., and Steele, B. C. H., 1982, "Effects of Inert Fillers on the Mechanical and Electrochemical Properties of Lithium Salt-Poly (Ethylene Oxide) Polymer Electrolytes," Solid State Ionics, **7**(1), pp. 75–79.
[30] Liang, G., Xu, J., Xu, W., Shen, X., Zhang, H., and Yao, M., 2011, "Effect of Filler-Polymer Interactions on the Crystalline Morphology of Peo-Based Solid Polymer Electrolytes by Y2o3 Nano-Fillers," Polym. Compos., **32**(4), pp. 511–518.
[31] Dirican, M., Yan, C., Zhu, P., and Zhang, X., 2019, "Composite Solid Electrolytes for All-Solid-State Lithium Batteries," Mater. Sci. Eng.: R: Rep., **136**, pp. 27–46.
[32] Larcht'e, F. C., and Cahn, J. L., 1982, "The Effect of Self-Stress on Diffusion in Solids," Acta Metall., **30**(10), pp. 1835–1845.
[33] Kelly, T., Moradi Ghadi, B., Berg, S., and Ardebili, H., 2016, "In Situ Study of Strain-Dependent Ion Conductivity of Stretchable Polyethylene Oxide Electrolyte," Sci. Rep., **6**(1), pp. 1–9.
[34] Mozaffari, K., Liu, L., and Sharma, P., 2021, "Theory of Soft Solid Electrolytes: Overall Properties of Composite Electrolytes, Effect of Deformation and Microstructural Design for Enhanced Ionic Conductivity," J. Mech. Phys. Solids, **158**(4), p. 104621.
[35] Xiao, Y., and Bhattacharya, K., 2008, "A Continuum Theory of Deformable, Semiconducting Ferroelectrics," Arch. Ration. Mech. Anal., **189**(1), pp. 59–95.
[36] Hong, W., Zhao, X., and Suo, Z., 2010, "Large Deformation and Electrochemistry of Polyelectrolyte Gels," J. Mech. Phys. Solids, **58**(4), pp. 558–577.
[37] Wang, X., and Hong, W., 2011, "Theory of Ionic Polymer Conductor Network Composite," Appl. Phys. Lett., **98**(8), p. 081910.
[38] Rejovitzky, E., Di Leo, C. V., and Anand, L., 2015, "A Theory and a Simulation Capability for the Growth of a Solid Electrolyte Interphase Layer At An Anode Particle in a Li-Ion Battery," J. Mech. Phys. Solids, **78**, pp. 210–230.
[39] Grazioli, D., Verners, O., Zadin, V., Brandell, D., and Simone, A., 2019, "Electrochemical-Mechanical Modeling of Solid Polymer Electrolytes: Impact of Mechanical Stresses on Li-Ion Battery Performance," Electrochim. Acta, **296**(8), pp. 1122–1141.
[40] Zhang, H., Dehghany, M., and Hu, Y., 2020, "Kinetics of Polyelectrolyte Gels," ASME J. Appl. Mech., **87**(6), p. 061010.
[41] Ganser, M., Hildebrand, F. E., Kamlah, M., and McMeeking, M., 2019, "A Finite Strain Electro-Chemo-Mechanical Theory for Ion Transport With Application to Binary Solid Electrolytes," J. Mech. Phys. Solids, **125**(1), pp. 681–713.
[42] Narayan, S., Stewart, E. M., and Anand, L., 2021, "Coupled Electro-Chemo-Elasticity: Application to Modeling the Actuation Response of Ionic Polymer–Metal Composites," J. Mech. Phys. Solids, **152**(4), p. 104394.
[43] Marshall, J., and Dayal, K., 2014, "Atomistic-to-Continuum Multiscale Modeling With Long-Range Electrostatic Interactions in Ionic Solids," J. Mech. Phys. Solids, **62**(6), pp. 137–162.
[44] Li, Q., and Ardebili, H., 2014, "Atomistic Investigation of the Nanoparticle Size and Shape Effects on Ionic Conductivity of Solid Polymer Electrolytes," Solid State Ionics, **268**, pp. 156–161.
[45] Sillamoni, I. J. C., and Idiart, M. I., 2015, "A Model Problem Concerning Ionic Transport in Microstructured Solid Electrolytes," Continuum Mech. Thermodyn., **27**(6), pp. 941–957.
[46] Liu, L., and Sharma, P., 2018, "Emergent Electromechanical Coupling of Electrets and Some Exact Relations–the Effective Properties of Soft Materials with Embedded External Charges and Dipoles," J. Mech. Phys. Solids, **112**(6), pp. 1–24.
[47] Rahmati, A. H., Yang, S., Bauer, S., and Sharma, P., 2019, "Nonlinear Bending Deformation of Soft Electrets and Prospects for Engineering Flexoelectricity and Transverse (d 31) Piezoelectricity," Soft Matter, **15**(1), pp. 127–148.
[48] Deng, Q., Liu, L., and Sharma, P., 2014, "Electrets in Soft Materials: Nonlinearity, Size Effects, and Giant Electromechanical Coupling," Phys. Rev. E, **90**(1), p. 012603.

[49] Sharma, P., Ganti, S., and Bhate, N., 2003, "Effect of Surfaces on the Size-Dependent Elastic State of Nano-Inhomogeneities," Appl. Phys. Lett., **82**(4), pp. 535–537.
[50] Sharma, P., and Ganti, S., 2004, "Size-Dependent Eshelby's Tensor for Embedded Nano-Inclusions Incorporating Surface/interface Energies," ASME J. Appl. Mech., **71**(5), pp. 663–671.
[51] Mozaffari, K., Yang, S., and Sharma, P., 2020, "Surface Energy and Nanoscale Mechanics," *Handbook of Materials Modeling: Applications: Current and Emerging Materials*, W. Andreoni and S. Yip, eds., Springer International Publishing, Cham, Switzerland, pp. 1949–1974.
[52] Sharma, P., 2004, "Size-Dependent Elastic Fields of Embedded Inclusions in Isotropic Chiral Solids," Int. J. Solids Struct., **41**(22–23), pp. 6317–6333.
[53] Zhang, X., and Sharma, P., 2005, "Inclusions and Inhomogeneities in Strain Gradient Elasticity With Couple Stresses and Related Problems," Int. J. Solids Struct., **42**(13), pp. 3833–3851.
[54] Natarajan, S., and Annabattula, R. K., 2019, "A Fenics Implementation of the Phase Field Method for Quasi-Static Brittle Fracture," Front. Struct. Civ. Eng., **13**(2), pp. 380–396.
[55] Siekierski, M., Wieczorek, W., and Nadara, K., 2007, "Mesoscale Models of Conductivity in Polymeric Electrolytes–A Comparative Study," Electrochim. Acta, **53**(4), pp. 1556–1567.
[56] Dasgupta, A., Sharma, P., and Upadhyayula, K., 2001, "Micro-Mechanics of Fatigue Damage in Pb-Sn Solder Due to Vibration and Thermal Cycling," Int. J. Damage Mech., **10**(2), pp. 101–132.